

Strange electromagnetic form factors of the nucleon with $N_f = 2 + 1$ $\mathcal{O}(a)$ -improved Wilson fermions

D. Djukanovic,¹ K. Ottnad,^{1,2} J. Wilhelm,² and H. Wittig^{1,2}

¹*Helmholtz Institute Mainz, Staudingerweg 18, D-55128 Mainz, Germany*

²*PRISMA+ Cluster of Excellence and Institute for Nuclear Physics,*

Johannes Gutenberg University of Mainz,

Johann-Joachim-Becher-Weg 45, D-55128 Mainz, Germany

(Dated: March 29, 2019)

Abstract

We present results for the strange contribution to the electromagnetic form factors of the nucleon computed on the CLS ensembles with $N_f = 2 + 1$ flavors of $\mathcal{O}(a)$ -improved Wilson fermions and an $\mathcal{O}(a)$ -improved vector current. Several source-sink separations are investigated in order to estimate the excited-state contamination. We calculate the form factors on six ensembles with lattice spacings in the range of $a = 0.049 - 0.086$ fm and pion masses in the range of $m_\pi = 200 - 360$ MeV, which allows for a controlled chiral and continuum extrapolation. In the computation of the quark-disconnected contributions we employ hierarchical probing as a variance reduction technique.

PACS numbers: 11.15.Ha, 12.38.Gc, 12.38.-t,

Keywords: Lattice QCD, Electromagnetic Form Factors, Strangeness

I. INTRODUCTION

The contributions of strange sea quarks to the nucleon electromagnetic form factors, which characterize the charge and current distribution in the nucleon, has been of high interest in the last decades. Experimentally, strange electromagnetic form factors can be measured through the parity-violating asymmetry, arising from the interference of the electromagnetic and neutral weak interactions, in the elastic scattering of polarized electrons on unpolarized protons. The first measurement by the SAMPLE experiment, at backward angles and low Q^2 , yielded a result for G_M^s which is consistent with zero [1]. The G0 collaboration combined measurements at forward and backward angles, and found a first indication of a non-zero G_E^s and G_M^s , contributing $\lesssim 10\%$ to the nucleon electromagnetic form factors [2, 3]. A first non-zero measurement has been obtained by the A4 experiment at MAMI with a four momentum transfer squared of $Q^2 = 0.22 \text{ GeV}^2$, where $G_E^s = 0.050 \pm 0.038 \pm 0.019$ and $G_M^s = -0.14 \pm 0.11 \pm 0.11$ [4]. A recent measurement from the HAPPEX collaboration at $Q^2 = 0.624 \text{ GeV}^2$ found a value for the combination of the strange electromagnetic form factors consistent with zero $G_E^s + 0.517 G_M^s = 0.003 \pm 0.010 \pm 0.004 \pm 0.009$ [5], confirming a previous measurement at $Q^2 = 0.48 \text{ GeV}^2$ where a value consistent with zero was found as well [6]. For a recent review of the experimental status of the strange electromagnetic form factors see [7].

On the theoretical side, Lattice QCD simulations allow for a non-perturbative determination of the strange nucleon form factors. This is a challenging calculation, due to the appearance of quark-disconnected diagrams, which are notoriously difficult to evaluate.¹ The most expensive part of the pertinent simulation is the calculation of the trace of an all-to-all propagator. In order to obtain a good signal, the application of variance-reduction techniques such as hierarchical probing [8] are crucial.

A prominent example to illustrate the importance of a precise knowledge of the strange nucleon form factors is the weak charge of the proton. At tree-level and without radiative corrections the weak charge is connected to the weak mixing angle through $Q_W(p) = 1 - 4 \sin^2 \theta_W$. Hence, through measurements of $Q_W(p)$, one can determine a fundamental parameter of the Standard Model. The experiment proceeds by measuring the parity-violating asymmetry, from which $Q_W(p)$ can be isolated provided that the required nucleon form factors to describe the hadronic contribution are known [7, 9]. Here the strange electromagnetic form factors G_E^s and G_M^s , as well as the strange axial form factor G_A^s , play a crucial role, as they constitute the leading uncertainty.

This paper closely follows the strategy outlined in [10] and is organized as follows. In Sec. II we give details on the setup of our calculation. Next we describe the extraction of strange nucleon form factors from nucleon correlation functions in Sec. III. A study of kaon mass and lattice spacing dependence is performed in Sec. IV. Finally, in Sec. V we present the extrapolation to the physical point of the strange electromagnetic form factors and conclude in Sec. VI.

II. SIMULATION DETAILS

We make use of the CLS $N_f = 2 + 1$ $\mathcal{O}(a)$ -improved Wilson fermion ensembles with the tree-level improved Lüscher-Weisz gauge action [11]. The fermion fields have open

¹ Note that the disconnected contribution cancels in the case of isovector form factors.

	β	a [fm]	$N_s^3 \times N_t$	m_π [MeV]	m_K [MeV]	m_N [MeV]	N_{cfg}	N_{meas}
H105	3.40	0.08636	$32^3 \times 96$	278	460	1037	1020	391680
N401*	3.46	0.07634	$48^3 \times 128$	289	462	1042	701	314048
N203	3.55	0.06426	$48^3 \times 128$	345	441	1111	772	345856
N200	3.55	0.06426	$48^3 \times 128$	283	463	1061	856	383488
D200	3.55	0.06426	$64^3 \times 128$	200	480	989	278	124544
N302*	3.70	0.04981	$48^3 \times 128$	354	458	1120	1177	527296

TABLE I. Gauge ensembles used in this work, where N_{cfg} denotes the number of gauge configurations and the last column corresponds to the total number of measurements for the ratio in Eq. (7). The values for the lattice spacing, pion and kaon masses are taken from [14], while the nucleon masses are estimated using the two point function in this work. For the ensembles marked with an asterisk the pion and kaon mass have been obtained from dedicated runs in connection with [15].

boundary conditions in time in order to prevent topological freezing [12]. Simulations have been performed such that the sum of the bare quark masses is constant, which implies a constant $\mathcal{O}(a)$ improved coupling [13]. See Tab. I for a list of ensembles used in this work².

We obtain the strange electromagnetic form factors of the nucleon by calculating the disconnected three-point function with a vector current insertion in the strange quark loop, which is explained in more detail in the next section. The relevant diagram and our chosen momentum setup is depicted in Fig. 1. The disconnected three-point function factorizes into separate traces for the strange quark loop and the nucleon two-point function

$$C_{3,V_\mu}^s(\mathbf{q}, z_0; \mathbf{p}', y_0, x; \Gamma_\nu) = \left\langle e^{-i\mathbf{q}\mathbf{x}} \mathcal{L}_{V_\mu}^s(\mathbf{q}, z_0) \cdot C_2(\mathbf{p}', y_0, x_0; \Gamma_\nu) \right\rangle_G, \quad (1)$$

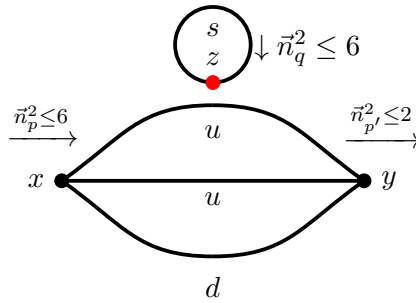


FIG. 1. Disconnected three-point function with a vector current inserted in the strange loop (red dot). For the range of momenta at the source and current insertion we use $\vec{n}_{p/q}^2 \leq 6$, while at the sink we restrict the range to $\vec{n}_{p'}^2 \leq 2$ ($\vec{n}_{p/q/p'}^2$ denote the units of squared lattice momenta).

² Note that the listed values of lattice spacing correspond to the values from [14] after a shift to $\phi_4 = 1.11$, while for the pion and kaon masses we quote the values at the ensemble value of ϕ_4 . See Ref. [14] for further details.

ensemble	N_{src}^{HP}	N_{src}^{LP}	time slices												
H105	4	32	24	▷	◁32	▷	◁40	▷	◁48	▷	◁56	▷	◁64	▷	◁72
otherwise	1	32	◁40	▷	◁48	▷	◁56	▷	◁64	▷	◁72	▷	◁80	▷	◁88

TABLE II. Source position for the calculation of the nucleon two-point function. The triangles illustrate the forward (▷) and the backward (◁) propagation of the nucleon. Time slices were chosen such that the effect of the boundary on the correlation functions is negligible.

where \mathcal{L}^s and C_2 denote the strange loop, given in Eq. (4), and the nucleon two-point function respectively.

The calculation of nucleon two-point functions C_2 proceeds via the standard nucleon interpolator

$$N_\alpha(x) = \epsilon_{abc} \left(u_\beta^a(x) (C\gamma_5)_{\beta\gamma} d_\gamma^b(x) \right) u_\alpha^c(x) , \quad (2)$$

and the parity projector $\Gamma_0 = \frac{1}{2}(1 + \gamma_0)$. Wuppertal smearing [16] is applied at the source and the sink for all quark propagators. We increase the statistics of the nucleon two-point function using the truncated solver method [17, 18]. The number of source positions per time slice for low (LP) and high (HP) precision solves and their distribution on different time slices of the lattice is given in Tab. II.

Traces over the strange quark loops can be stochastically estimated using four-dimensional noise vectors η . For a local current

$$V^s = \bar{s}(x)\Gamma s(x) \quad (3)$$

the trace over the strange quark loop then reads

$$\langle \mathcal{L}_I^s(\mathbf{q}, z_0) \rangle_G = - \sum_{\mathbf{z} \in \Lambda} e^{i\mathbf{q} \cdot \mathbf{z}} \langle \text{tr} [S^s(z; z) \Gamma] \rangle_G = - \sum_{\mathbf{z} \in \Lambda} e^{i\mathbf{q} \cdot \mathbf{z}} \langle \eta^\dagger(z) \Gamma \psi(z) \rangle_{G, \eta} , \quad (4)$$

with

$$D^s \psi = \eta, \quad (5)$$

where D^s denotes the Dirac operator for the strange quark, and the sum is taken over the spatial volume Λ . Instead of a local current we consider the $\mathcal{O}(a)$ -improved conserved vector current in this work

$$V_\mu(z)^{\text{Imp.}} = \frac{1}{2} \left(\bar{s}(z + \hat{\mu}a)(1 + \gamma_\mu)U_\mu(z)^\dagger s(z) - \bar{s}(z)(1 - \gamma_\mu)U_\mu(z)s(z + \hat{\mu}a) \right) + ac_V \partial_\nu (\bar{s}(z)\sigma_{\mu\nu}s(z)) , \quad (6)$$

with the improvement coefficient c_V taken from [19]. Furthermore we use hierarchical probing [8], which replaces the sequence of noise vectors by one noise vector multiplied with a sequence of Hadamard vectors. We find a large reduction of the statistical error of the strange loop for 512 Hadamard vectors compared to the estimate using 512 $U(1)$ noise vectors (see Fig. 2). This number of Hadamard vectors coincides with distance-4 probing, i.e. contributions to the variance of the trace of neighboring lattice sites up to distance 4 are removed [8]. While not necessarily required for the present study, the quark loops have

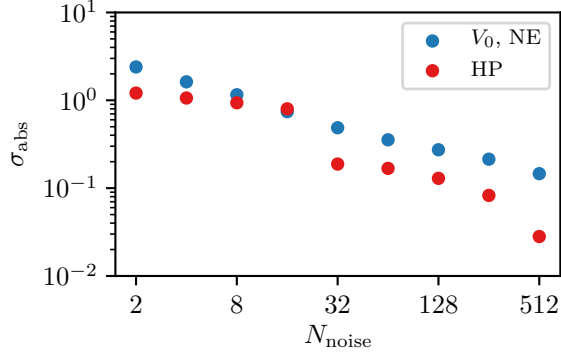


FIG. 2. Comparison of the absolute error of the strange loop on ensemble H105 with vector insertion V_0 calculated with the naive estimator (NE) and hierarchical probing (HP), for which we set the number of noise vectors (N_{noise}) equal to the number of Hadamard vectors (N_{had}). A reduction in the error by an order of magnitude is observed for $N_{\text{had}} = 512$.

been generated with two stochastic sources to allow also for the calculation of other quark-disconnected contributions for future projects. The quark loops in this study were obtained by averaging two independent noise vectors with 512 Hadamard vectors each. This amounts to a total of 1024 inversions per gauge configuration for the strange loop calculation.

III. EXTRACTING FORM FACTORS FROM LATTICE QCD

To extract the strange contribution to the electromagnetic form factors of the nucleon we consider the ratios (see [20–22])

$$R_{V_\mu}^s(z_0, \mathbf{q}; y_0, \mathbf{p}'; \Gamma_\nu) = \frac{C_{3,V_\mu}^s(\mathbf{q}, z_0; \mathbf{p}', y_0; \Gamma_\nu)}{C_2(\mathbf{p}', y_0)} \sqrt{\frac{C_2(\mathbf{p}', y_0)C_2(\mathbf{p}', z_0)C_2(\mathbf{p}'-\mathbf{q}, y_0-z_0)}{C_2(\mathbf{p}'-\mathbf{q}, y_0)C_2(\mathbf{p}'-\mathbf{q}, z_0)C_2(\mathbf{p}', y_0-z_0)}}. \quad (7)$$

Performing the spectral decomposition and only taking the ground state into account, these ratios read

$$R_{V_\mu}^s(z_0, \mathbf{q}; y_0, \mathbf{p}'; \Gamma_\nu) \xrightarrow{z_0, (y_0-z_0) \rightarrow \infty} \frac{1}{4\sqrt{(E_{\mathbf{p}'-\mathbf{q}} + m)(E_{\mathbf{p}'} + m)E_{\mathbf{p}'}E_{\mathbf{p}'-\mathbf{q}}}} T\left(\tilde{V}_\mu^s, \Gamma_\nu, \mathbf{q}, \mathbf{p}'\right), \quad (8)$$

$$T\left(\tilde{V}_\mu^s, \Gamma_\nu, \mathbf{q}, \mathbf{p}'\right) = \text{tr} \left[\Gamma_\nu (E_{\mathbf{p}'}\gamma_0 - i\mathbf{p}'\boldsymbol{\gamma} + m) \tilde{V}_\mu^s(\mathbf{q}) (E_{\mathbf{p}'-\mathbf{q}}\gamma_0 - i(\mathbf{p}' - \mathbf{q})\boldsymbol{\gamma} + m) \right], \quad (9)$$

where \tilde{V}_μ^s can be obtained using the parametrization of the nucleon matrix element ³

$$\langle N, \mathbf{k}, s | V^\mu(x) | N, \mathbf{k}', s' \rangle = \bar{u}^s(\mathbf{k}) \left(\gamma^\mu F_1(Q^2) + i\sigma^{\mu\nu} \frac{q_\nu}{2m} F_2(Q^2) \right) u^{s'}(\mathbf{k}') e^{iq \cdot x}. \quad (10)$$

We proceed by evaluating the trace in Eq. (9) for four different projectors

$$\Gamma_0 = \frac{1}{2}(1 + \gamma_0) \quad , \quad \Gamma_k = \Gamma_0 i\gamma_5\gamma_k \quad , \quad k \in \{1, 2, 3\} \quad , \quad (11)$$

³ For completeness we have collected the explicit expressions for Eq. (9) in App. A.

combined with all components of the vector current \tilde{V}_μ^s , leading to the asymptotic behavior of the ratios in the following form

$$R_{V_\mu}^s(z_0, \mathbf{q}; y_0, \mathbf{p}'; \Gamma_\nu) \xrightarrow{z_0, (y_0 - z_0) \rightarrow \infty} M_{\mu\nu}^E(\mathbf{q}, \mathbf{p}') G_E^s(Q^2) + M_{\mu\nu}^M(\mathbf{q}, \mathbf{p}') G_M^s(Q^2). \quad (12)$$

By analogy with Ref. [23] we collect all kinematic prefactors $M_{\mu\nu}^E$ and $M_{\mu\nu}^M$ at a common Q^2 into a matrix M and write the ratios as a vector \mathbf{R} , which results in a (generally) overdetermined system of equations for the form factors \mathbf{G}

$$M \mathbf{G} = \mathbf{R} \quad ; \quad M = \begin{pmatrix} M_1^E & M_1^M \\ \vdots & \vdots \\ M_N^E & M_N^M \end{pmatrix}, \quad \mathbf{G} = \begin{pmatrix} G_E^s \\ G_M^s \end{pmatrix}, \quad \mathbf{R} = \begin{pmatrix} R_1 \\ \vdots \\ R_N \end{pmatrix}. \quad (13)$$

The system can be solved by minimizing the least-squares function

$$\chi^2 = (\mathbf{R} - M\mathbf{G})^T C^{-1} (\mathbf{R} - M\mathbf{G}). \quad (14)$$

Note that we neglect all equations with vanishing kinematical factors ($M^E = M^M = 0$) and average equivalent equations, i.e. with identical M^E and M^M . The latter average can already be carried out at the level of the nucleon three-point functions, where the momenta of the nucleon states at the source and the sink of the three-point functions are related by spatial symmetry [24]. In addition, averaging the nucleon two-point functions over equivalent momentum classes, we construct the ratios in Eq. (7) from these averaged correlation functions. Solving the system of equations at each z_0 and y_0 leads to the so-called effective form factors, which still suffer from excited-state contamination. Following Refs. [16, 25–27] we obtain an estimate of the asymptotic value of the form factors using the summation method with source-sink separations in the range of $y_0 = 0.5 - 1.3$ fm. The effect of excited-state contamination is illustrated in Fig. 3, where we compare estimates from plateau fits to the summation method. In the case of the magnetic form factor, the plateau estimates show a clear trend towards the results obtained using the summation method. For the electric form factor both methods agree already at small values of y_0 . The effective form factors for several source-sink separations are also shown. No significant deviation from a plateau around the midpoint is visible.

IV. KAON MASS AND LATTICE SPACING DEPENDENCE

In Figures 4 and 5 we show estimates of the electric and magnetic form factors as a function of Q^2 and for ensembles corresponding to different kaon masses. We will use the summation method data as our standard dataset, since it is less affected by excited-state contamination, compared to the plateau fits. Nevertheless we include the analysis of the plateau data, for a conservative choice of source-sink separation of 1 fm using 5 points around the midpoint, as an estimate for the uncertainty coming from excited states. In order to further analyze the kaon mass and lattice spacing dependence we use model independent z -expansion fits [28, 29] to fifth order to extract the radii and magnetic moment⁴. The form

⁴ We have explicitly checked that going to a maximum order of 10 does not change the fit results.

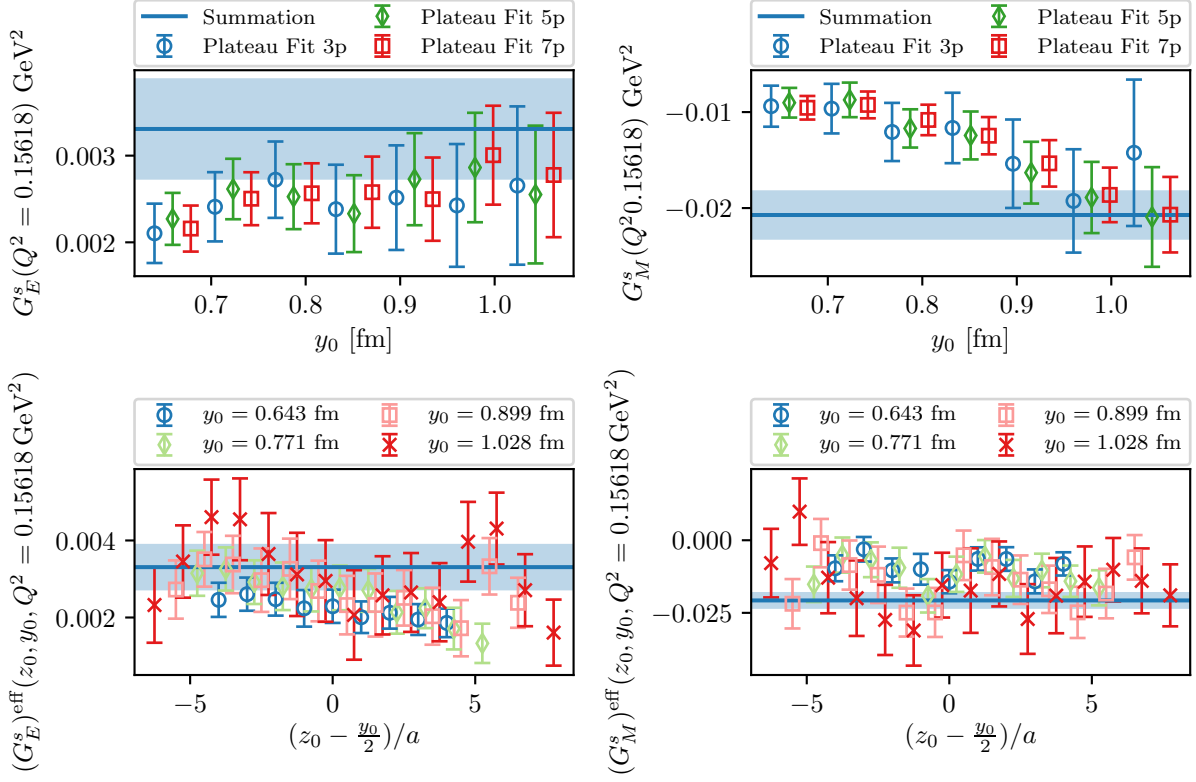


FIG. 3. (top) Illustration of the excited-state contamination for ensemble N200. We show three variations of the plateau estimate, using fitting ranges of the central three (3p), five (5p) or seven (7p) data points of the effective form factors. (bottom) Results for the effective form factors determined via Eq. (13) compared to the estimate derived from the summation method (horizontal band).

factors can be expanded as

$$G_{E/M}(Q^2) = \sum_{k=1/0}^5 a_k^{E/M} z(Q^2)^k, \quad z(Q^2) = \frac{\sqrt{t_{\text{cut}} + Q^2} - \sqrt{t_{\text{cut}}}}{\sqrt{t_{\text{cut}} + Q^2} + \sqrt{t_{\text{cut}}}}. \quad (15)$$

Since the physical ω and ϕ mesons are narrow resonances and because one cannot easily establish whether or not they are unstable particles on the analyzed ensembles, we use $4m_K^2$ for the value of the cut in the z -expansion, where we use the ensemble kaon mass for m_K (see Tab. I). We stabilize the fits using Gaussian priors centered around zero for all coefficients with $k > 1$. To this end we first determine the coefficients $a_{0,1}$ from a fit without priors, and subsequently use the maximum of these coefficients to estimate the width of the priors, i.e. $a_{k>1} = 0 \pm c \times \max\{|a_0|, |a_1|\}$. We find that for $c = 5$ the extraction of the radii and the magnetic moment are stable and lead to consistent results even after applying a cut of $Q^2 < 0.5 \text{ GeV}^2$ (see Fig. 6). Finally we estimate the effect of this choice on the final observables by repeating the analysis with the prior width doubled.

From the z -expansion fits we can extract the strange magnetic moment μ^s , as well as the

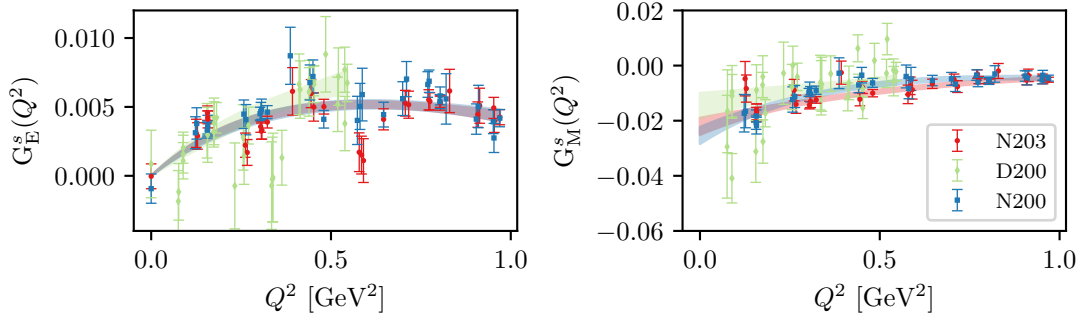


FIG. 4. Kaon mass dependence of the strange electromagnetic form factors at a fixed lattice spacing $a = 0.064$ fm, where we show the summation method data together with model independent z -expansion fits to the data.

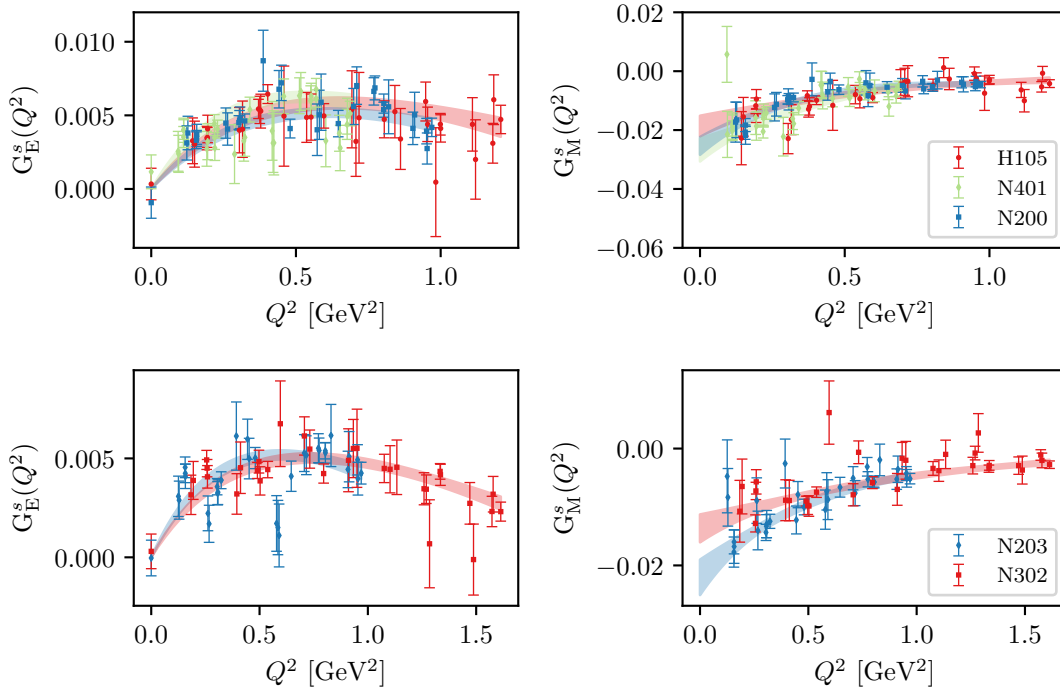


FIG. 5. Lattice spacing dependence of the strange electromagnetic form factors at pion mass $m_\pi = 280$ MeV (top) and $m_\pi = 340$ MeV (bottom), where we show the summation method data together with model independent z -expansion fits to the data.

electric and magnetic charge radii $(r_{E/M}^2)^s$,

$$\mu^s = a_0^M, \quad (16)$$

$$(r_{E/M}^2)^s = -\frac{3}{2t_{\text{cut}}} a_1^{E/M}. \quad (17)$$

We have repeated the analysis in several variations in order to assess systematic errors, and subsequently perform chiral and continuum extrapolations. Since the radii and magnetic

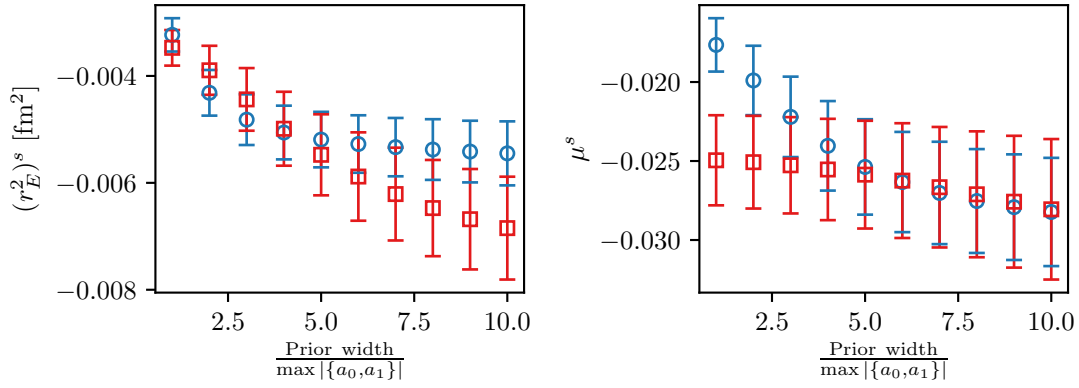


FIG. 6. Dependence of the electric radius (left) and magnetic moment (right) on the prior width in units of $\max\{|a_0, a_1|\}$ for the summation method on ensemble N200, where the squares and circles denote fits with and without a cut in the momentum transfer ($Q^2 < 0.5 \text{ GeV}^2$) respectively.

moments are defined at $Q^2 = 0$ we perform the fits applying a cut of $Q^2 < 0.5 \text{ GeV}^2$ and treat the difference to fitting all of the data as a systematic uncertainty. This cut also ensures that all ensembles contribute over the whole range in Q^2 .

In total we thus have four sets of values for the radii and magnetic moments for every ensemble, for which we analyze the lattice spacing and kaon mass dependence in the next section.

V. CHIRAL AND CONTINUUM EXTRAPOLATION

The analyzed set of ensembles allow for a controlled chiral and continuum extrapolation of the strange electromagnetic form factors. In the following we will investigate the kaon mass dependence⁵ using

$$\begin{aligned} (r_E^2)^s(m_K) &= c_1 + c_2 \log(m_K) + \tilde{c}_1 a^2, \\ \mu^s(m_K) &= c_3 + c_4 m_K + \tilde{c}_2 a^2, \\ (r_M^2)^s(m_K) &= \frac{c_5}{m_K} + c_6 + \tilde{c}_3 a^2, \end{aligned} \quad (18)$$

which is derived from SU(3) HBChPT [30] with additional terms describing the dependence on the lattice spacing a . Here the kaon mass dependence of the strange quark current is given via kaon loops exclusively. Note that the radii are divergent in the limit of massless kaons. Strictly speaking the term c_6 is of higher order in the chiral expansion. However since our data for the magnetic radius does not show the divergent behavior expected from HBChPT (see Fig. 7), we amend the expressions from [30] by this term. Such a promotion of a higher order term, especially for the magnetic radius, was also found in HBChPT in Ref. [31].

⁵ Note that the CLS ensembles follow the $\text{tr } M_q = \text{constant}$ trajectory, the kaon mass and the pion mass are therefore not varied independently.

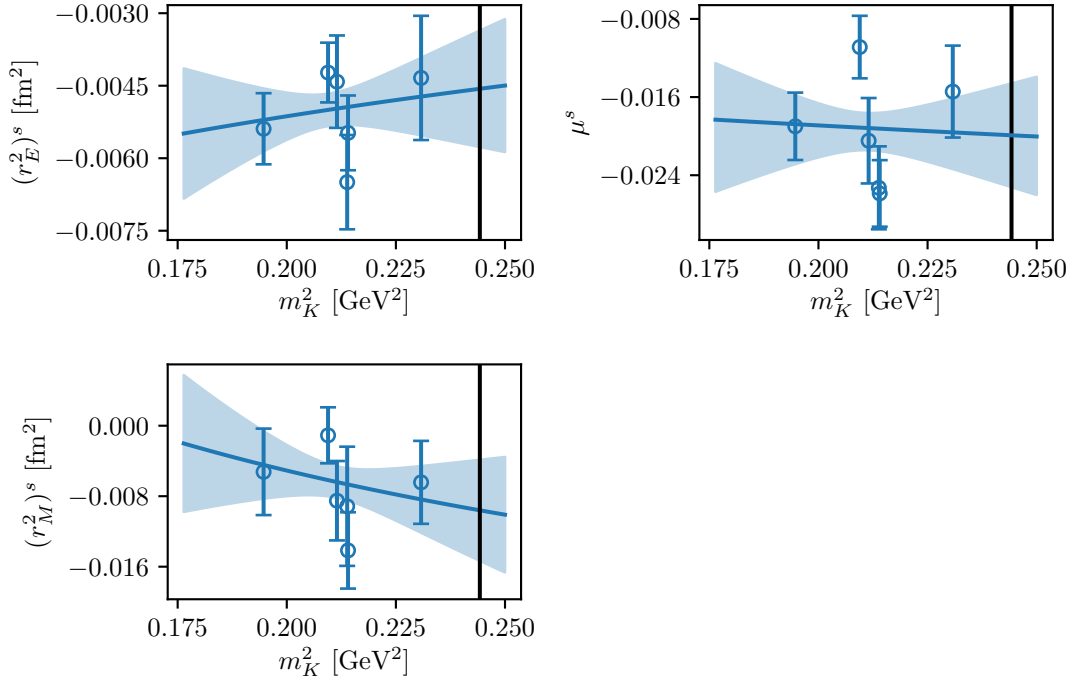


FIG. 7. Chiral and continuum extrapolation of the electric and magnetic radius and magnetic moment, using the standard method of Tab. III. The vertical line denotes the physical kaon mass in the isospin limit [35].

For each of the variations of the z -expansion fit in the previous section we analyze the chiral behavior separately. The chirally extrapolated values for the standard fit procedure and the variations of the z -expansion fits performed to assess systematic uncertainties are given in Tab. III. We treat the difference of the central values for the variations as an estimate for a (symmetric) systematic error. In addition we perform a fit including lattice artifacts to the standard z -expansion fit. Comparing the AIC_c , i.e. the Akaike information criterion [32] adjusted for small sample size [33, 34], we find that the fits including lattice spacing give larger values, by at least 27 using the maximum likelihood estimator for the sample variance, i.e. the fits omitting $\mathcal{O}(a^2)$ are favored. We therefore quote the fit without lattice artifacts as our best value, using the difference in the central value for the two procedures as a systematic error from finite lattice spacing. The finite volume effects are exponentially suppressed, and given $m_\pi L \gtrsim 4$ on our ensembles we neglect these contributions.

At the physical point we find⁶

$$(r_E^2)_{\text{phys}}^s = -0.0046(12)(7)(1)(9)(6) \text{ fm}^2, \quad (19)$$

$$\mu_{\text{phys}}^s = -0.020(5)(0)(2)(11)(3), \quad (20)$$

$$(r_M^2)_{\text{phys}}^s = -0.010(6)(2)(5)(7)(2) \text{ fm}^2, \quad (21)$$

as our final estimate, where the first error is statistical and the remaining errors come from the variations in the fitting procedure given in Tab. III.

⁶ For the kaon mass we use the value in the isospin limit $m_K = 0.4942$ GeV [35].

Fit	$(r_E^2)^2$ [fm ²]	μ^s	$(r_M^2)^s$ [fm ²]	χ^2/DOF
Standard	-0.0046(12)	-0.020(5)	-0.010(6)	1.27, 3.34, 1.52
Doubling prior width	-0.0053(15)	-0.020(6)	-0.012(8)	1.24, 2.28, 0.90
Plateau method	-0.0045(14)	-0.022(8)	-0.014(8)	1.49, 1.87, 1.49
Including $\mathcal{O}(a^2)$	-0.0036(16)	-0.009(7)	-0.003(8)	1.43, 2.89, 1.41
No cut in Q^2	-0.0051(9)	-0.017(5)	-0.008(5)	3.15, 3.70, 2.58

TABLE III. Fit results for the standard fit and variations thereof. In the last column the three values indicate the reduced χ^2 of the electric radius, the magnetic moment and the magnetic radius respectively, where the number of degrees of freedom is 4 (3) in each fit without (with) lattice artifacts.

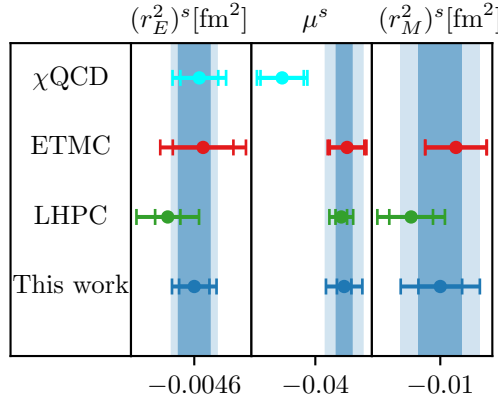


FIG. 8. Comparison of our final values for the radii and magnetic moments with LHPC [36], ETMC [37] and χ QCD [38], where the dark and light blue bands describe the statistical error and the total error including systematics respectively.

For the radii our values are in good agreement with other lattice determinations [36–38]. Our value for the magnetic moment is again in good agreement with [36, 37]. The magnetic moment from [38] disagrees with our estimate and with [36, 37] by more than two standard deviations, see Fig. 8. Our best estimate of the radii and magnetic moment compare favorably to the available experimental data, as can be seen from Fig. 9.

VI. SUMMARY AND CONCLUSION

In this study, we have reported on our calculation of the strange contribution to the electromagnetic form factors obtained on six CLS $N_f = 2 + 1$ $\mathcal{O}(a)$ -improved Wilson fermion ensembles. For the calculation of the disconnected contributions we use the method of hierarchical probing which significantly reduces the statistical error. We obtain the strange form factors on each ensemble at 32 different values of Q^2 by solving an overdetermined system of equations. To deal with excited state contamination we employ the summation method. We find agreement with plateau estimates for large enough source-sink separations. The strange charge radii and the strange magnetic moment are obtained on each ensemble through model independent z -expansion fits, and later extrapolated to the physical point. Our results are

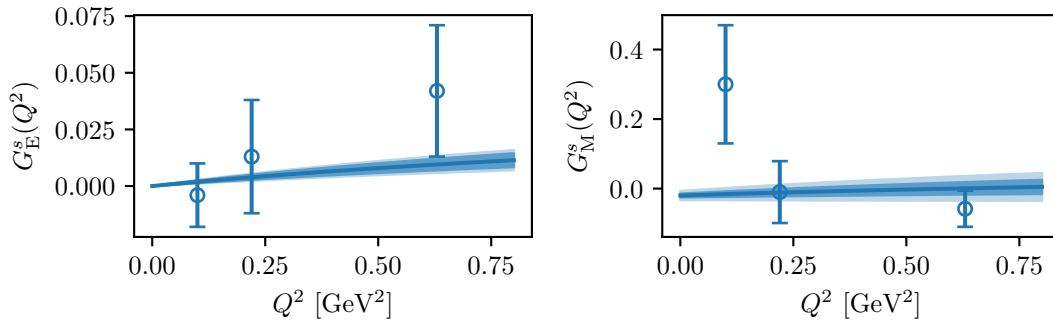


FIG. 9. Comparison of our standard fit, based on the z -expansion up to $k = 1$, to the analysis of existing experimental data [7]. The dark and light blue bands describe the statistical error and the total error including systematics respectively.

compatible with other Lattice QCD studies and in good agreement to experimental data.

With the current set of ensembles, the physical values for the strange charge radii and the strange magnetic moment still have large relative statistical errors. We aim to improve this, by enlarging the number of ensembles.

ACKNOWLEDGMENTS

We thank H. Meyer and G. von Hippel for useful discussions and comments. This research is supported by the DFG through the SFB 1044. K.O. is supported by the Deutsche Forschungsgemeinschaft (DFG, German Research Foundation) grant HI 2048/1-1. Additionally, this work has been supported by the Cluster of Excellence Precision Physics, Fundamental Interactions, and Structure of Matter (PRISMA⁺ EXC 2118/1) funded by the German Research Foundation (DFG) within the German Excellence Strategy (Project ID 39083149). Calculations for this project were partly performed on the HPC clusters "Clover" and "HIMster II" at the Helmholtz-Institut Mainz and "Mogon II" at JGU Mainz. Additional computer time has been allocated through projects HMZ21 and HMZ36 on the Blue-Gene supercomputer system "JUQUEEN" at NIC, Jülich. Our programs use the QDP++ library [39] and deflated SAP+GCR solver from the openQCD package [40], while the contractions have been explicitly checked using [41]. We are grateful to our colleagues in the CLS initiative for sharing ensembles.

Appendix A: Kinematic Prefactors

Here we give the explicit formulas for the traces in Eq. (9), from which the kinematic prefactors $M_{\mu\nu}^E$ and $M_{\mu\nu}^M$ in Eq. (12) are obtained.

$$\begin{aligned}
\frac{1}{4}T \left(\tilde{V}_0^s, \Gamma_0, \mathbf{q}, \mathbf{p}' \right) &= \frac{F_1^s(Q^2)}{2} [(E_{\mathbf{p}'-\mathbf{q}} + m)(E_{\mathbf{p}'} + m) + \mathbf{p}'(\mathbf{p}' - \mathbf{q})] \\
&\quad + \frac{F_2^s(Q^2)}{4m} [E_{\mathbf{p}'} \mathbf{q}(\mathbf{p}' - \mathbf{q}) - E_{\mathbf{p}'-\mathbf{q}} \mathbf{p}'\mathbf{q} - m\mathbf{q}^2] \\
\frac{1}{4}T \left(\tilde{V}_i^s, \Gamma_0, \mathbf{q}, \mathbf{p}' \right) &= -\frac{iF_1^s(Q^2)}{2} [(E_{\mathbf{p}'-\mathbf{q}} + m) p_i + (E_{\mathbf{p}'} + m) (\mathbf{p}' - \mathbf{q})_i] \\
&\quad + \frac{iF_2^s(Q^2)}{4m} [p_i (q_0(E_{\mathbf{p}'-\mathbf{q}} + m) - \mathbf{q}(\mathbf{p}' - \mathbf{q})) \\
&\quad \quad - (\mathbf{p}' - \mathbf{q})_i (q_0(E_{\mathbf{p}'} + m) - \mathbf{q}\mathbf{p}')] \\
\frac{1}{4}T \left(\tilde{V}_0^s, \Gamma_i, \mathbf{q}, \mathbf{p}' \right) &= \frac{iF_1^s(Q^2)}{2} [(\mathbf{p}' \times \mathbf{q})_i] \\
&\quad + \frac{iF_2^s(Q^2)}{4m} [(E_{\mathbf{p}'} + E_{\mathbf{p}'-\mathbf{q}} + 2m) (\mathbf{p}' \times \mathbf{q})_i] \\
\frac{1}{4}T \left(\tilde{V}_i^s, \Gamma_i, \mathbf{q}, \mathbf{p}' \right) &= -\frac{F_2^s(Q^2)}{4m} [(2\mathbf{p}' - \mathbf{q})_i (\mathbf{p}' \times \mathbf{q})_i] \\
\frac{1}{4}T \left(\tilde{V}_j^s, \Gamma_i, \mathbf{q}, \mathbf{p}' \right) &= \frac{F_1^s(Q^2)}{2} [(E_{\mathbf{p}'-\mathbf{q}} + m) \mathbf{p}'(\mathbf{e}_j \times \mathbf{e}_i) - (E_{\mathbf{p}'} + m) (\mathbf{p}' - \mathbf{q})(\mathbf{e}_j \times \mathbf{e}_i)] \\
&\quad + \frac{F_2^s(Q^2)}{4m} [-(2m(E_{\mathbf{p}'} + m) + p_j (2\mathbf{p}' - \mathbf{q})_j) (\mathbf{p}' - \mathbf{q})(\mathbf{e}_j \times \mathbf{e}_i) \\
&\quad \quad + (2m(E_{\mathbf{p}'-\mathbf{q}} + m) + (\mathbf{p}' - \mathbf{q})_j (2\mathbf{p}' - \mathbf{q})_j) \mathbf{p}'(\mathbf{e}_j \times \mathbf{e}_i)]
\end{aligned} \tag{A1}$$

Here the last equation relies on $i \neq j$, where $i, j \in \{1, 2, 3\}$. We always relate the Pauli and Dirac form factor F_1^s and F_2^s to the Sachs form factors

$$G_E^s(Q^2) = F_1^s(Q^2) - \frac{Q^2}{4m^2} F_2^s(Q^2) , \tag{A2}$$

$$G_M^s(Q^2) = F_1^s(Q^2) + F_2^s(Q^2) . \tag{A3}$$

Appendix B: Tables

In this section we give the extracted form factors $G_{E/M}$ as well as the z -expansion fits for the final result quoted in the main text.

H105	G_E^s		G_M^s	
a_k	Summation Method	Plateau Fit	Summation Method	Plateau Fit
0	-	-	-0.02047 (0.00437)	-0.01233 (0.00599)
1	0.06397 (0.01385)	0.06823 (0.01405)	0.12329 (0.06527)	0.04532 (0.07789)
2	0.02234 (0.14166)	-0.02693 (0.14610)	-0.00992 (0.28592)	0.00175 (0.23002)
3	0.00627 (0.15825)	-0.00133 (0.16380)	-0.00232 (0.28851)	0.00026 (0.23533)
4	0.00108 (0.15816)	0.00019 (0.16458)	-0.00038 (0.28453)	0.00002 (0.23424)
5	0.00015 (0.15918)	0.00006 (0.16606)	-0.00005 (0.28363)	-0.00000 (0.23054)
χ^2/dof	0.44508	1.64311	1.46231	0.48937

TABLE IV. Fit of the z -expansion to the strange electromagnetic form factors on ensemble H105 with a transferred four-momentum cut of $Q^2 < 0.5 \text{ GeV}^2$.

N401	G_E^s		G_M^s	
a_k	Summation Method	Plateau Fit	Summation Method	Plateau Fit
0	-	-	-0.02529 (0.00425)	-0.02095 (0.00435)
1	0.09512 (0.01429)	0.10383 (0.01443)	0.13391 (0.09905)	0.13431 (0.08529)
2	-0.27623 (0.16770)	-0.30477 (0.16933)	0.13998 (0.62712)	-0.04352 (0.48865)
3	-0.02203 (0.25734)	-0.03529 (0.26595)	0.01803 (0.67666)	-0.01013 (0.49372)
4	-0.00082 (0.25992)	-0.00313 (0.26699)	0.00121 (0.68362)	-0.00160 (0.49435)
5	0.00007 (0.25824)	-0.00025 (0.26746)	-0.00001 (0.67480)	-0.00021 (0.49920)
χ^2/dof	1.73239	1.16637	1.47959	0.96105

TABLE V. Fit of the z -expansion to the strange electromagnetic form factors on ensemble N401 with a transferred four-momentum cut of $Q^2 < 0.5 \text{ GeV}^2$.

N203	G_E^s		G_M^s	
a_k	Summation Method	Plateau Fit	Summation Method	Plateau Fit
0	-	-	-0.01899 (0.00345)	-0.01435 (0.00458)
1	0.07188 (0.00981)	0.06983 (0.01178)	0.06979 (0.06544)	0.02585 (0.06573)
2	-0.24568 (0.09677)	-0.22658 (0.11057)	0.00194 (0.34785)	-0.03506 (0.28291)
3	-0.03558 (0.15444)	-0.03115 (0.14710)	-0.00407 (0.36546)	-0.00927 (0.28600)
4	-0.00422 (0.15360)	-0.00345 (0.14939)	-0.00127 (0.37107)	-0.00165 (0.28557)
5	-0.00049 (0.15529)	-0.00037 (0.14689)	-0.00025 (0.37221)	-0.00025 (0.28763)
χ^2/dof	1.89473	1.84721	1.71021	1.18630

TABLE VI. Fit of the z -expansion to the strange electromagnetic form factors on ensemble N203 with a transferred four-momentum cut of $Q^2 < 0.5 \text{ GeV}^2$.

N200	G_E^s		G_M^s	
a_k	Summation Method	Plateau Fit	Summation Method	Plateau Fit
0	-	-	-0.02586 (0.00341)	-0.02665 (0.00517)
1	0.08026 (0.01134)	0.06574 (0.01291)	0.20748 (0.06348)	0.23425 (0.06965)
2	-0.34096 (0.11673)	-0.19624 (0.13298)	-0.16836 (0.34266)	-0.04257 (0.23831)
3	-0.06001 (0.15726)	-0.03532 (0.16129)	-0.04070 (0.35692)	-0.01019 (0.24036)
4	-0.00831 (0.15976)	-0.00498 (0.16238)	-0.00670 (0.35371)	-0.00166 (0.23809)
5	-0.00106 (0.15881)	-0.00064 (0.16369)	-0.00094 (0.35217)	-0.00023 (0.23128)
χ^2/dof	1.69598	0.96513	0.96210	1.88794

TABLE VII. Fit of the z -expansion to the strange electromagnetic form factors on ensemble N200 with a transferred four-momentum cut of $Q^2 < 0.5 \text{ GeV}^2$.

D200	G_E^s		G_M^s	
a_k	Summation Method	Plateau Fit	Summation Method	Plateau Fit
0	-	-	-0.01544 (0.00470)	-0.01214 (0.00862)
1	0.06857 (0.02031)	0.06464 (0.02218)	0.10160 (0.07439)	0.09163 (0.13288)
2	-0.01483 (0.22268)	-0.14348 (0.24059)	-0.06996 (0.37373)	-0.00272 (0.63158)
3	0.00768 (0.31098)	-0.01647 (0.28613)	-0.01276 (0.36976)	0.00061 (0.64526)
4	0.00191 (0.30663)	-0.00143 (0.28985)	-0.00165 (0.36929)	0.00019 (0.64590)
5	0.00030 (0.30945)	-0.00010 (0.28545)	-0.00019 (0.37093)	0.00003 (0.65096)
χ^2/dof	1.05330	1.14854	1.77733	0.59909

TABLE VIII. Fit of the z -expansion to the strange electromagnetic form factors on ensemble D200 with a transferred four-momentum cut of $Q^2 < 0.5 \text{ GeV}^2$.

N302	G_E^s		G_M^s	
a_k	Summation Method	Plateau Fit	Summation Method	Plateau Fit
0	-	-	-0.01088 (0.00320)	-0.00910 (0.00515)
1	0.06065 (0.00886)	0.05927 (0.01035)	0.01563 (0.04561)	0.00821 (0.06148)
2	-0.13785 (0.07965)	-0.18502 (0.09230)	-0.00556 (0.19990)	-0.00875 (0.19448)
3	-0.02385 (0.09626)	-0.03279 (0.10684)	-0.00165 (0.19593)	-0.00221 (0.19935)
4	-0.00316 (0.09728)	-0.00449 (0.10823)	-0.00033 (0.19528)	-0.00038 (0.20066)
5	-0.00038 (0.09759)	-0.00056 (0.11077)	-0.00005 (0.19247)	-0.00006 (0.19969)
χ^2/dof	2.72651	1.64723	1.55374	2.20057

TABLE IX. Fit of the z -expansion to the strange electromagnetic form factors on ensemble N302 with a transferred four-momentum cut of $Q^2 < 0.5 \text{ GeV}^2$.

H105	G_E^s		G_M^s	
Q^2 [GeV ²]	Summation Method	Plateau Fit	Summation Method	Plateau Fit
0.00000	0.00034 (0.00107)	0.00135 (0.00106)	-	-
0.14300	0.00327 (0.00155)	0.00195 (0.00233)	-0.02275 (0.00903)	-0.00662 (0.01681)
0.14974	0.00304 (0.00156)	0.00585 (0.00197)	-0.01549 (0.00658)	-0.00950 (0.01191)
0.19268	0.00346 (0.00080)	0.00378 (0.00077)	-0.01174 (0.00267)	-0.00795 (0.00374)
0.19397	0.00350 (0.00067)	0.00383 (0.00069)	-0.01517 (0.00226)	-0.01139 (0.00306)
0.19487	0.00408 (0.00093)	0.00557 (0.00113)	-0.00947 (0.00324)	-0.01279 (0.00545)
0.30464	0.00399 (0.00154)	0.00532 (0.00211)	-0.02289 (0.00514)	-0.02235 (0.00939)
0.31545	0.00406 (0.00191)	0.00576 (0.00275)	-0.01645 (0.00510)	-0.02176 (0.01025)
0.37069	0.00544 (0.00065)	0.00423 (0.00081)	-0.00832 (0.00166)	-0.00677 (0.00251)
0.37505	0.00537 (0.00093)	0.00592 (0.00124)	-0.01291 (0.00269)	-0.01148 (0.00406)
0.37833	0.00529 (0.00115)	0.00605 (0.00188)	-0.01197 (0.00295)	-0.00765 (0.00611)
0.40252	0.00644 (0.00064)	0.00666 (0.00076)	-0.00987 (0.00148)	-0.00880 (0.00213)
0.45865	0.00495 (0.00340)	0.00744 (0.00375)	-0.01160 (0.00850)	-0.01750 (0.01360)
0.53690	0.00486 (0.00170)	0.00337 (0.00243)	-0.00795 (0.00313)	-0.01109 (0.00592)
0.55227	0.00488 (0.00157)	0.00524 (0.00189)	-0.00937 (0.00308)	-0.00146 (0.00521)
0.59650	0.00496 (0.00083)	0.00458 (0.00094)	-0.00896 (0.00172)	-0.00855 (0.00219)
0.69338	0.00541 (0.00262)	0.00305 (0.00435)	-0.00433 (0.00486)	0.01567 (0.00764)
0.70727	0.00323 (0.00238)	-0.00021 (0.00309)	-0.00360 (0.00459)	-0.00018 (0.00773)
0.71798	0.00484 (0.00308)	0.00288 (0.00441)	-0.00341 (0.00528)	0.00410 (0.01151)
0.80515	0.00473 (0.00126)	0.00472 (0.00158)	-0.00471 (0.00199)	-0.00449 (0.00308)
0.84184	0.00525 (0.00178)	0.00582 (0.00258)	0.00120 (0.00339)	-0.00045 (0.00599)
0.86127	0.00340 (0.00207)	0.00559 (0.00252)	-0.00265 (0.00363)	-0.00752 (0.00603)
0.94815	0.00594 (0.00132)	0.00857 (0.00204)	-0.00082 (0.00227)	-0.00067 (0.00427)
0.95489	0.00439 (0.00117)	0.00710 (0.00166)	-0.00245 (0.00190)	-0.00146 (0.00349)
0.98315	0.00046 (0.00370)	0.00405 (0.00415)	-0.00748 (0.00583)	-0.00590 (0.00838)
0.99902	0.00440 (0.00073)	0.00557 (0.00086)	-0.00336 (0.00108)	-0.00403 (0.00162)
1.00001	0.00411 (0.00093)	0.00390 (0.00127)	-0.00285 (0.00143)	0.00055 (0.00260)
1.10979	0.00439 (0.00182)	0.00403 (0.00232)	-0.00636 (0.00258)	-0.00900 (0.00425)
1.12050	0.00200 (0.00270)	0.00614 (0.00378)	-0.01003 (0.00381)	-0.00675 (0.00683)
1.18020	0.00310 (0.00135)	0.00278 (0.00207)	-0.00531 (0.00177)	-0.00186 (0.00353)
1.18347	0.00606 (0.00169)	0.00209 (0.00272)	-0.00069 (0.00232)	0.00083 (0.00451)
1.20767	0.00472 (0.00096)	0.00397 (0.00134)	-0.00422 (0.00133)	-0.00342 (0.00189)

TABLE X. Results for the strange electromagnetic form factors from the summation method and plateau fit at 1 fm on ensemble H105.

N401	G_E^s		G_M^s	
Q^2 [GeV ²]	Summation Method	Plateau Fit	Summation Method	Plateau Fit
0.00000	0.00116 (0.00115)	0.00176 (0.00112)	-	-
0.09297	0.00256 (0.00135)	0.00255 (0.00128)	0.00571 (0.00949)	-0.01468 (0.01318)
0.09455	0.00238 (0.00126)	0.00284 (0.00123)	-0.02148 (0.00782)	-0.01459 (0.00972)
0.11160	0.00353 (0.00072)	0.00371 (0.00072)	-0.01811 (0.00394)	-0.02243 (0.00448)
0.11190	0.00404 (0.00066)	0.00366 (0.00063)	-0.02018 (0.00337)	-0.01543 (0.00396)
0.11209	0.00399 (0.00082)	0.00418 (0.00087)	-0.01899 (0.00413)	-0.01054 (0.00517)
0.19208	0.00273 (0.00118)	0.00442 (0.00109)	-0.01577 (0.00571)	-0.01013 (0.00684)
0.19485	0.00321 (0.00122)	0.00517 (0.00125)	-0.01864 (0.00481)	-0.01690 (0.00558)
0.21804	0.00444 (0.00061)	0.00543 (0.00059)	-0.02050 (0.00219)	-0.01470 (0.00280)
0.21904	0.00349 (0.00081)	0.00563 (0.00080)	-0.01587 (0.00311)	-0.01153 (0.00379)
0.21983	0.00278 (0.00085)	0.00412 (0.00091)	-0.01489 (0.00374)	-0.00720 (0.00490)
0.22895	0.00407 (0.00061)	0.00495 (0.00059)	-0.01420 (0.00214)	-0.01249 (0.00234)
0.28782	0.00237 (0.00200)	0.00585 (0.00184)	-0.02224 (0.00656)	-0.01464 (0.00727)
0.31993	0.00327 (0.00138)	0.00644 (0.00127)	-0.01616 (0.00366)	-0.01296 (0.00478)
0.32360	0.00350 (0.00128)	0.00694 (0.00118)	-0.01782 (0.00372)	-0.00876 (0.00433)
0.34084	0.00539 (0.00084)	0.00640 (0.00079)	-0.01255 (0.00228)	-0.00853 (0.00258)
0.41775	0.00395 (0.00200)	0.00430 (0.00184)	-0.00471 (0.00469)	-0.01755 (0.00620)
0.42102	0.00312 (0.00200)	0.00509 (0.00184)	-0.00454 (0.00446)	-0.00760 (0.00546)
0.42380	0.00313 (0.00218)	0.00520 (0.00212)	-0.00826 (0.00454)	-0.01159 (0.00641)
0.45789	0.00629 (0.00118)	0.00684 (0.00114)	-0.00927 (0.00283)	-0.00828 (0.00338)
0.51211	0.00633 (0.00122)	0.00475 (0.00110)	-0.00534 (0.00317)	-0.00501 (0.00336)
0.51687	0.00663 (0.00129)	0.00522 (0.00116)	-0.00912 (0.00287)	-0.00603 (0.00326)
0.55086	0.00599 (0.00102)	0.00509 (0.00096)	-0.00268 (0.00249)	-0.00478 (0.00300)
0.55255	0.00631 (0.00087)	0.00620 (0.00086)	-0.00577 (0.00193)	-0.00728 (0.00233)
0.56979	0.00614 (0.00059)	0.00550 (0.00062)	-0.00607 (0.00147)	-0.00421 (0.00169)
0.56999	0.00677 (0.00074)	0.00662 (0.00076)	-0.00809 (0.00164)	-0.00626 (0.00201)
0.60319	0.00327 (0.00176)	0.00315 (0.00167)	-0.00668 (0.00370)	-0.00463 (0.00425)
0.64997	0.00378 (0.00122)	0.00377 (0.00117)	-0.00705 (0.00261)	-0.00771 (0.00304)
0.65275	0.00278 (0.00154)	0.00343 (0.00152)	-0.01197 (0.00331)	-0.00859 (0.00380)
0.67693	0.00438 (0.00102)	0.00455 (0.00098)	-0.00664 (0.00194)	-0.00372 (0.00247)
0.67772	0.00494 (0.00122)	0.00396 (0.00131)	-0.00835 (0.00248)	-0.00954 (0.00295)
0.68694	0.00512 (0.00083)	0.00558 (0.00082)	-0.00497 (0.00157)	-0.00342 (0.00184)

TABLE XI. Results for the strange electromagnetic form factors from the summation method and plateau fit at 1 fm on ensemble N401.

N203	G_E^s		G_M^s	
Q^2 [GeV ²]	Summation Method	Plateau Fit	Summation Method	Plateau Fit
0.00000	-0.00003 (0.00090)	-0.00153 (0.00112)	-	-
0.12555	0.00308 (0.00102)	0.00534 (0.00123)	-0.00476 (0.00624)	-0.01342 (0.01149)
0.12876	0.00289 (0.00096)	0.00532 (0.00121)	-0.00834 (0.00493)	-0.00039 (0.00845)
0.15658	0.00455 (0.00052)	0.00515 (0.00069)	-0.01772 (0.00258)	-0.01591 (0.00487)
0.15718	0.00425 (0.00047)	0.00481 (0.00064)	-0.01598 (0.00204)	-0.01474 (0.00295)
0.15758	0.00409 (0.00062)	0.00502 (0.00080)	-0.01677 (0.00288)	-0.01592 (0.00403)
0.26184	0.00222 (0.00088)	0.00105 (0.00118)	-0.00891 (0.00390)	-0.00484 (0.00568)
0.26716	0.00169 (0.00094)	0.00067 (0.00140)	-0.01402 (0.00331)	-0.01198 (0.00512)
0.30442	0.00357 (0.00041)	0.00337 (0.00062)	-0.01435 (0.00139)	-0.01170 (0.00233)
0.30633	0.00324 (0.00059)	0.00231 (0.00079)	-0.01329 (0.00197)	-0.01114 (0.00295)
0.30794	0.00329 (0.00063)	0.00271 (0.00089)	-0.01292 (0.00233)	-0.01139 (0.00356)
0.32310	0.00390 (0.00043)	0.00321 (0.00057)	-0.01245 (0.00121)	-0.01160 (0.00188)
0.39291	0.00613 (0.00172)	0.00528 (0.00219)	-0.00256 (0.00419)	0.00367 (0.00728)
0.44463	0.00597 (0.00102)	0.00611 (0.00127)	-0.01222 (0.00238)	-0.01587 (0.00502)
0.45196	0.00499 (0.00103)	0.00509 (0.00128)	-0.00788 (0.00224)	-0.00743 (0.00363)
0.48029	0.00502 (0.00053)	0.00530 (0.00070)	-0.01001 (0.00134)	-0.01118 (0.00212)
0.57851	0.00171 (0.00141)	0.00175 (0.00165)	-0.01045 (0.00336)	-0.01087 (0.00506)
0.58494	0.00150 (0.00137)	0.00270 (0.00165)	-0.00732 (0.00319)	-0.00271 (0.00468)
0.59036	0.00110 (0.00159)	0.00381 (0.00209)	-0.00874 (0.00341)	-0.00602 (0.00521)
0.64631	0.00410 (0.00077)	0.00378 (0.00100)	-0.00662 (0.00169)	-0.00473 (0.00264)
0.70667	0.00527 (0.00093)	0.00570 (0.00117)	-0.00508 (0.00198)	-0.00962 (0.00344)
0.71601	0.00516 (0.00098)	0.00564 (0.00138)	-0.00762 (0.00214)	-0.01061 (0.00351)
0.77185	0.00552 (0.00073)	0.00506 (0.00099)	-0.00312 (0.00159)	-0.00774 (0.00256)
0.77507	0.00540 (0.00063)	0.00481 (0.00094)	-0.00526 (0.00130)	-0.00642 (0.00214)
0.80349	0.00538 (0.00041)	0.00513 (0.00058)	-0.00574 (0.00086)	-0.00660 (0.00139)
0.80389	0.00528 (0.00052)	0.00488 (0.00076)	-0.00573 (0.00102)	-0.00721 (0.00167)
0.82990	0.00616 (0.00157)	0.00483 (0.00182)	-0.00194 (0.00270)	-0.00748 (0.00448)
0.90814	0.00444 (0.00092)	0.00313 (0.00121)	-0.00523 (0.00175)	-0.00332 (0.00258)
0.91347	0.00509 (0.00127)	0.00514 (0.00177)	-0.00354 (0.00226)	0.00169 (0.00355)
0.95264	0.00493 (0.00076)	0.00517 (0.00097)	-0.00426 (0.00117)	-0.00516 (0.00192)
0.95424	0.00397 (0.00083)	0.00330 (0.00116)	-0.00509 (0.00151)	-0.00626 (0.00235)
0.96941	0.00425 (0.00055)	0.00417 (0.00072)	-0.00515 (0.00090)	-0.00531 (0.00147)

TABLE XII. Results for the strange electromagnetic form factors from the summation method and plateau fit at 1 fm on ensemble N203.

N200	G_E^s		G_M^s	
Q^2 [GeV ²]	Summation Method	Plateau Fit	Summation Method	Plateau Fit
0.00000	-0.00093 (0.00106)	-0.00055 (0.00139)	-	-
0.12293	0.00313 (0.00116)	0.00204 (0.00161)	-0.01729 (0.00681)	-0.02589 (0.01542)
0.12665	0.00380 (0.00114)	0.00154 (0.00163)	-0.01656 (0.00600)	0.00015 (0.01105)
0.15618	0.00331 (0.00057)	0.00255 (0.00079)	-0.02071 (0.00244)	-0.02093 (0.00519)
0.15678	0.00343 (0.00054)	0.00320 (0.00073)	-0.01831 (0.00221)	-0.02165 (0.00364)
0.15728	0.00371 (0.00068)	0.00297 (0.00097)	-0.02179 (0.00303)	-0.02532 (0.00509)
0.25772	0.00447 (0.00103)	0.00183 (0.00147)	-0.01230 (0.00460)	-0.01697 (0.00803)
0.26375	0.00407 (0.00110)	0.00205 (0.00175)	-0.01123 (0.00402)	-0.01699 (0.00742)
0.30282	0.00451 (0.00047)	0.00403 (0.00063)	-0.00973 (0.00144)	-0.00647 (0.00297)
0.30513	0.00467 (0.00066)	0.00365 (0.00092)	-0.00858 (0.00259)	-0.00497 (0.00401)
0.30693	0.00483 (0.00073)	0.00300 (0.00122)	-0.01039 (0.00279)	-0.01177 (0.00512)
0.32310	0.00462 (0.00047)	0.00445 (0.00063)	-0.00893 (0.00149)	-0.00491 (0.00246)
0.38688	0.00871 (0.00207)	0.00502 (0.00265)	-0.00277 (0.00558)	0.00434 (0.00987)
0.44152	0.00677 (0.00127)	0.00548 (0.00154)	-0.00705 (0.00280)	-0.01500 (0.00559)
0.44985	0.00721 (0.00120)	0.00418 (0.00160)	-0.00347 (0.00281)	0.00084 (0.00495)
0.47998	0.00410 (0.00064)	0.00359 (0.00090)	-0.00628 (0.00161)	-0.00191 (0.00270)
0.57339	0.00402 (0.00175)	0.00546 (0.00223)	-0.00395 (0.00415)	0.00219 (0.00841)
0.58082	0.00504 (0.00167)	0.00810 (0.00215)	-0.00824 (0.00379)	-0.00954 (0.00637)
0.58695	0.00590 (0.00191)	0.00857 (0.00279)	-0.00484 (0.00420)	-0.00907 (0.00725)
0.64631	0.00444 (0.00090)	0.00471 (0.00120)	-0.00543 (0.00189)	-0.00710 (0.00335)
0.69934	0.00560 (0.00123)	0.00744 (0.00153)	-0.00483 (0.00234)	-0.00775 (0.00467)
0.71008	0.00702 (0.00127)	0.00810 (0.00172)	-0.00672 (0.00268)	-0.00389 (0.00479)
0.76924	0.00663 (0.00093)	0.00643 (0.00129)	-0.00345 (0.00192)	-0.00493 (0.00360)
0.77296	0.00686 (0.00081)	0.00734 (0.00116)	-0.00603 (0.00164)	-0.00675 (0.00297)
0.80309	0.00538 (0.00051)	0.00581 (0.00074)	-0.00520 (0.00100)	-0.00521 (0.00187)
0.80359	0.00580 (0.00065)	0.00610 (0.00098)	-0.00561 (0.00123)	-0.00451 (0.00226)
0.82016	0.00558 (0.00183)	0.00182 (0.00251)	-0.00303 (0.00299)	-0.00551 (0.00552)
0.90403	0.00412 (0.00110)	0.00443 (0.00154)	-0.00377 (0.00190)	-0.00580 (0.00341)
0.91005	0.00503 (0.00154)	0.00296 (0.00233)	-0.00446 (0.00257)	-0.00640 (0.00468)
0.95133	0.00393 (0.00086)	0.00253 (0.00126)	-0.00525 (0.00139)	-0.00716 (0.00247)
0.95324	0.00275 (0.00106)	0.00381 (0.00157)	-0.00352 (0.00180)	-0.01072 (0.00386)
0.96941	0.00418 (0.00063)	0.00349 (0.00094)	-0.00456 (0.00108)	-0.00367 (0.00185)

TABLE XIII. Results for the strange electromagnetic form factors from the summation method and plateau fit at 1 fm on ensemble N200.

D200	G_E^s		G_M^s	
Q^2 [GeV ²]	Summation Method	Plateau Fit	Summation Method	Plateau Fit
0.00000	0.00086 (0.00245)	0.00279 (0.00314)	-	-
0.07543	-0.00185 (0.00223)	0.00058 (0.00316)	-0.02945 (0.01863)	-0.02786 (0.03715)
0.07653	-0.00117 (0.00205)	0.00005 (0.00278)	-0.01659 (0.01504)	-0.01260 (0.02745)
0.08889	0.00109 (0.00132)	0.00313 (0.00165)	-0.04089 (0.00895)	-0.01793 (0.01775)
0.08899	0.00204 (0.00113)	0.00281 (0.00140)	-0.01097 (0.00774)	-0.01581 (0.01209)
0.08919	0.00157 (0.00137)	0.00168 (0.00191)	-0.00955 (0.00956)	-0.01169 (0.01477)
0.15527	0.00327 (0.00198)	0.00306 (0.00254)	-0.03115 (0.01122)	-0.02594 (0.01966)
0.15708	0.00298 (0.00199)	0.00419 (0.00258)	-0.00891 (0.00922)	-0.00692 (0.01470)
0.17406	0.00319 (0.00110)	0.00288 (0.00132)	-0.00706 (0.00460)	0.00191 (0.00896)
0.17466	0.00421 (0.00143)	0.00558 (0.00179)	-0.00402 (0.00758)	0.00724 (0.01104)
0.17516	0.00381 (0.00156)	0.00458 (0.00206)	-0.02756 (0.00786)	-0.02037 (0.01349)
0.18179	0.00421 (0.00111)	0.00455 (0.00129)	-0.01730 (0.00493)	-0.00671 (0.00716)
0.23251	-0.00073 (0.00312)	0.00008 (0.00429)	-0.00278 (0.01129)	-0.00205 (0.01903)
0.25591	0.00279 (0.00238)	0.00499 (0.00335)	-0.00777 (0.00821)	-0.02576 (0.01537)
0.25832	0.00143 (0.00205)	-0.00023 (0.00281)	0.00007 (0.00698)	-0.00774 (0.01103)
0.27078	0.00365 (0.00134)	0.00386 (0.00203)	-0.00409 (0.00497)	-0.01025 (0.00781)
0.33485	-0.00071 (0.00318)	0.00230 (0.00447)	-0.00616 (0.00991)	0.00424 (0.01819)
0.33696	-0.00027 (0.00308)	0.00356 (0.00401)	-0.00806 (0.00987)	0.00327 (0.01494)
0.33877	-0.00012 (0.00322)	0.00295 (0.00441)	-0.00677 (0.00981)	-0.00817 (0.01694)
0.36358	0.00131 (0.00199)	0.00179 (0.00264)	-0.00295 (0.00648)	-0.00256 (0.00979)
0.41129	0.00664 (0.00220)	0.00348 (0.00334)	-0.01137 (0.00504)	0.00449 (0.01013)
0.41430	0.00626 (0.00208)	0.00286 (0.00291)	-0.00628 (0.00610)	0.00222 (0.01017)
0.43901	0.00609 (0.00176)	0.00149 (0.00250)	0.00627 (0.00490)	-0.00887 (0.00899)
0.44001	0.00696 (0.00142)	0.00384 (0.00199)	-0.00716 (0.00403)	0.00015 (0.00635)
0.45257	0.00690 (0.00110)	0.00290 (0.00159)	-0.00840 (0.00306)	-0.00460 (0.00514)
0.45267	0.00664 (0.00132)	0.00448 (0.00199)	-0.01535 (0.00388)	-0.00104 (0.00621)
0.48521	0.00882 (0.00274)	0.01279 (0.00343)	0.00182 (0.00625)	0.00848 (0.01126)
0.51875	0.00518 (0.00197)	0.01002 (0.00237)	-0.00284 (0.00512)	0.00437 (0.00758)
0.52056	0.00720 (0.00208)	0.00733 (0.00290)	0.00961 (0.00570)	0.02815 (0.00982)
0.53814	0.00770 (0.00164)	0.01075 (0.00218)	-0.00167 (0.00408)	0.01878 (0.00710)
0.53874	0.00379 (0.00197)	0.01119 (0.00243)	-0.00565 (0.00533)	-0.00720 (0.00865)
0.54527	0.00674 (0.00136)	0.00909 (0.00167)	-0.00219 (0.00337)	0.00405 (0.00543)

TABLE XIV. Results for the strange electromagnetic form factors from the summation method and plateau fit at 1 fm on ensemble D200.

N302	G_E^s		G_M^s	
Q^2 [GeV ²]	Summation Method	Plateau Fit	Summation Method	Plateau Fit
0.00000	0.00030 (0.00088)	0.00098 (0.00099)	-	-
0.18358	0.00316 (0.00099)	0.00582 (0.00153)	-0.01073 (0.00529)	-0.01557 (0.01293)
0.19423	0.00389 (0.00096)	0.00541 (0.00149)	-0.00649 (0.00469)	-0.01593 (0.00961)
0.25587	0.00492 (0.00048)	0.00460 (0.00060)	-0.01281 (0.00146)	-0.01527 (0.00273)
0.25800	0.00451 (0.00044)	0.00433 (0.00051)	-0.00725 (0.00148)	-0.00468 (0.00223)
0.25955	0.00407 (0.00057)	0.00425 (0.00081)	-0.00570 (0.00209)	-0.00661 (0.00381)
0.39513	0.00320 (0.00102)	0.00322 (0.00141)	-0.00884 (0.00350)	0.00210 (0.00711)
0.41206	0.00453 (0.00130)	0.00395 (0.00192)	-0.00889 (0.00346)	-0.00603 (0.00786)
0.49006	0.00439 (0.00041)	0.00363 (0.00052)	-0.00899 (0.00084)	-0.00878 (0.00167)
0.49732	0.00484 (0.00058)	0.00400 (0.00078)	-0.00973 (0.00155)	-0.00706 (0.00284)
0.50264	0.00386 (0.00071)	0.00247 (0.00107)	-0.00983 (0.00176)	-0.00365 (0.00384)
0.53787	0.00444 (0.00041)	0.00428 (0.00049)	-0.00747 (0.00090)	-0.00889 (0.00143)
0.59593	0.00675 (0.00216)	0.00583 (0.00305)	0.00616 (0.00541)	-0.00440 (0.01034)
0.70713	0.00613 (0.00097)	0.00583 (0.00125)	-0.00791 (0.00189)	-0.01123 (0.00383)
0.73200	0.00547 (0.00096)	0.00735 (0.00146)	-0.00064 (0.00195)	-0.00920 (0.00419)
0.79587	0.00423 (0.00048)	0.00471 (0.00065)	-0.00583 (0.00102)	-0.00616 (0.00164)
0.91055	0.00491 (0.00159)	0.00083 (0.00207)	-0.00699 (0.00272)	-0.00274 (0.00540)
0.93290	0.00550 (0.00147)	0.00451 (0.00199)	-0.00165 (0.00271)	0.00121 (0.00500)
0.94984	0.00551 (0.00198)	0.00179 (0.00320)	-0.00200 (0.00323)	0.00658 (0.00784)
1.07564	0.00449 (0.00072)	0.00409 (0.00094)	-0.00340 (0.00118)	-0.00387 (0.00201)
1.10255	0.00445 (0.00119)	0.00464 (0.00151)	-0.00378 (0.00184)	-0.00328 (0.00371)
1.13381	0.00455 (0.00138)	0.00466 (0.00202)	-0.00100 (0.00243)	0.00017 (0.00494)
1.25922	0.00347 (0.00081)	0.00439 (0.00119)	-0.00292 (0.00142)	0.00069 (0.00290)
1.26987	0.00344 (0.00072)	0.00409 (0.00118)	-0.00077 (0.00117)	0.00009 (0.00262)
1.28477	0.00068 (0.00222)	0.00171 (0.00280)	0.00267 (0.00330)	0.00946 (0.00590)
1.33364	0.00434 (0.00039)	0.00437 (0.00055)	-0.00344 (0.00062)	-0.00381 (0.00109)
1.33519	0.00417 (0.00053)	0.00478 (0.00084)	-0.00288 (0.00083)	-0.00004 (0.00174)
1.47077	0.00273 (0.00105)	0.00411 (0.00151)	-0.00292 (0.00149)	-0.00302 (0.00283)
1.48771	-0.00011 (0.00179)	-0.00035 (0.00295)	-0.00368 (0.00239)	0.00510 (0.00520)
1.57297	0.00232 (0.00077)	0.00360 (0.00105)	-0.00110 (0.00091)	0.00059 (0.00197)
1.57829	0.00319 (0.00090)	0.00326 (0.00155)	-0.00203 (0.00125)	-0.00076 (0.00287)
1.61351	0.00231 (0.00048)	0.00331 (0.00070)	-0.00276 (0.00064)	-0.00264 (0.00120)

TABLE XV. Results for the strange electromagnetic form factors from the summation method and plateau fit at 1 fm on ensemble N302.

-
- [1] D. T. Spayde et al. (SAMPLE), Phys. Lett. **B583**, 79 (2004), nucl-ex/0312016.
 - [2] D. Androić, D. S. Armstrong, J. Arvieux, S. L. Bailey, D. H. Beck, E. J. Beise, J. Benesch, F. Benmokhtar, L. Bimbot, J. Birchall, et al. (G0 Collaboration), Phys. Rev. Lett. **104**, 012001 (2010), URL <https://link.aps.org/doi/10.1103/PhysRevLett.104.012001>.
 - [3] D. S. Armstrong, J. Arvieux, R. Asaturyan, T. Averett, S. L. Bailey, G. Batigne, D. H. Beck, E. J. Beise, J. Benesch, L. Bimbot, et al. (G0 Collaboration), Phys. Rev. Lett. **95**, 092001 (2005), URL <https://link.aps.org/doi/10.1103/PhysRevLett.95.092001>.
 - [4] S. Baunack, K. Aulenbacher, D. Balaguer Ríos, L. Capozza, J. Diefenbach, B. Gläser, D. von Harrach, Y. Imai, E.-M. Kabuß, R. Kothe, et al., Phys. Rev. Lett. **102**, 151803 (2009), URL <https://link.aps.org/doi/10.1103/PhysRevLett.102.151803>.
 - [5] Z. Ahmed, K. Allada, K. A. Aniol, D. S. Armstrong, J. Arrington, P. Baturin, V. Bellini, J. Benesch, R. Beminiwattha, F. Benmokhtar, et al. (HAPPEX Collaboration), Phys. Rev. Lett. **108**, 102001 (2012), URL <https://link.aps.org/doi/10.1103/PhysRevLett.108.102001>.
 - [6] K. A. Aniol et al. (HAPPEX), Phys. Rev. **C69**, 065501 (2004), nucl-ex/0402004.
 - [7] F. E. Maas and K. D. Paschke, Prog. Part. Nucl. Phys. **95**, 209 (2017).
 - [8] A. Stathopoulos, J. Laeuchli, and K. Orginos (2013), 1302.4018.
 - [9] D. Becker et al., Eur. Phys. J. **A54**, 208 (2018), 1802.04759.
 - [10] D. Djukanovic, H. Meyer, K. Ottnad, G. von Hippel, J. Wilhelm, and H. Wittig, in *36th International Symposium on Lattice Field Theory (Lattice 2018) East Lansing, MI, United States, July 22-28, 2018* (2018), 1810.10810.
 - [11] M. Bruno, D. Djukanovic, G. P. Engel, A. Francis, G. Herdoiza, H. Horch, P. Korcyl, T. Korzec, M. Papinutto, S. Schaefer, et al., Journal of High Energy Physics **2015**, 43 (2015), ISSN 1029-8479, URL [https://doi.org/10.1007/JHEP02\(2015\)043](https://doi.org/10.1007/JHEP02(2015)043).
 - [12] M. Lüscher and S. Schaefer, JHEP **07**, 036 (2011), 1105.4749.
 - [13] W. Bietenholz, V. Bornyakov, N. Cundy, M. Göckeler, R. Horsley, A. Kennedy, W. Lockhart, Y. Nakamura, H. Perlt, D. Pleiter, et al., Physics Letters B **690**, 436 (2010), ISSN 0370-2693, URL <http://www.sciencedirect.com/science/article/pii/S0370269310006702>.
 - [14] M. Bruno, T. Korzec, and S. Schaefer, Phys. Rev. **D95**, 074504 (2017), 1608.08900.
 - [15] M. C, A. Grardin, K. Ottnad, and H. B. Meyer, PoS **LATTICE2018**, 137 (2018), 1811.08669.
 - [16] S. Güsken, Nucl. Phys. Proc. Suppl. **17**, 361 (1990).
 - [17] G. Bali, S. Collins, A. Frommer, K. Kahl, I. Kanamori, B. Müller, M. Rottmann, and J. Simeth, PoS **LATTICE2015**, 350 (2015), 1509.06865.
 - [18] E. Shintani, R. Arthur, T. Blum, T. Izubuchi, C. Jung, and C. Lehner, Phys. Rev. D **91**, 114511 (2015), URL <https://link.aps.org/doi/10.1103/PhysRevD.91.114511>.
 - [19] A. Gérardin, T. Harris, and H. B. Meyer, Phys. Rev. D **99**, 014519 (2019), URL <https://link.aps.org/doi/10.1103/PhysRevD.99.014519>.
 - [20] C. Alexandrou, T. Korzec, G. Koutsou, M. Brinet, J. Carbonell, V. Drach, P.-A. Harraud, and R. Baron (European Twisted Mass), PoS **LATTICE2008**, 139 (2008), 0811.0724.
 - [21] J. R. Green, J. W. Negele, A. V. Pochinsky, S. N. Syritsyn, M. Engelhardt, and S. Krieg, Phys. Rev. **D90**, 074507 (2014), 1404.4029.
 - [22] S. Capitani, M. Della Morte, D. Djukanovic, G. von Hippel, J. Hua, B. Jger, B. Knippschild, H. B. Meyer, T. D. Rae, and H. Wittig, Phys. Rev. **D92**, 054511 (2015), 1504.04628.

- [23] S. Capitani, M. Della Morte, D. Djukanovic, G. M. von Hippel, J. Hua, B. Jäger, P. M. Junnarkar, H. B. Meyer, T. D. Rae, and H. Wittig, *Int. J. Mod. Phys. A* **34**, 1950009 (2019), 1705.06186, URL <https://doi.org/10.1142/S0217751X1950009X>.
- [24] S. N. Syritsyn, J. D. Bratt, M. F. Lin, H. B. Meyer, J. W. Negele, A. V. Pochinsky, M. Procura, M. Engelhardt, P. Hägler, T. R. Hemmert, et al. (LHPC Collaboration), *Phys. Rev. D* **81**, 034507 (2010), URL <https://link.aps.org/doi/10.1103/PhysRevD.81.034507>.
- [25] L. Maiani, G. Martinelli, M. L. Paciello, and B. Taglienti, *Nucl. Phys. B* **293**, 420 (1987).
- [26] T. Doi, M. Deka, S.-J. Dong, T. Draper, K.-F. Liu, D. Mankame, N. Mathur, and T. Streuer, *Phys. Rev. D* **80**, 094503 (2009), 0903.3232.
- [27] B. B. Brandt, S. Capitani, M. Della Morte, D. Djukanovic, J. Gegelia, G. von Hippel, A. Jüttner, B. Knippschild, H. B. Meyer, and H. Wittig, *Eur. Phys. J. ST* **198**, 79 (2011), 1106.1554.
- [28] R. J. Hill and G. Paz, *Phys. Rev. D* **82**, 113005 (2010), URL <https://link.aps.org/doi/10.1103/PhysRevD.82.113005>.
- [29] Z. Epstein, G. Paz, and J. Roy, *Phys. Rev. D* **90**, 074027 (2014), URL <https://link.aps.org/doi/10.1103/PhysRevD.90.074027>.
- [30] T. R. Hemmert, B. Kubis, and U.-G. Meissner, *Phys. Rev. C* **60**, 045501 (1999), nucl-th/9904076.
- [31] H. W. Hammer, S. J. Puglia, M. J. Ramsey-Musolf, and S.-L. Zhu, *Phys. Lett. B* **562**, 208 (2003), hep-ph/0206301.
- [32] H. Akaike, in *Proc. 2nd International Symposium on Information Theory*, (Eds. B. N. Petrov and F. Csaki), *Akademiai Kiado, Budapest* (1973), pp. 267–281.
- [33] N. Sugiura, *Communications in Statistics - Theory and Methods* **7**, 13 (1978), <https://doi.org/10.1080/03610927808827599>, URL <https://doi.org/10.1080/03610927808827599>.
- [34] C. M. Hurvich and C.-L. Tsai, *Biometrika* **76**, 297 (1989), ISSN 0006-3444, <http://oup.prod.sis.lan/biomet/article-pdf/76/2/297/737009/76-2-297.pdf>, URL <https://dx.doi.org/10.1093/biomet/76.2.297>.
- [35] S. Aoki et al., *Eur. Phys. J. C* **77**, 112 (2017), 1607.00299.
- [36] J. Green, S. Meinel, M. Engelhardt, S. Krieg, J. Laeuchli, J. Negele, K. Orginos, A. Pochinsky, and S. Syritsyn, *Phys. Rev. D* **92**, 031501 (2015), 1505.01803.
- [37] C. Alexandrou, M. Constantinou, K. Hadjiyiannakou, K. Jansen, C. Kallidonis, G. Koutsou, and A. Vaquero Avilés-Casco, *Phys. Rev. D* **97**, 094504 (2018), 1801.09581.
- [38] R. S. Sufian, Y.-B. Yang, J. Liang, T. Draper, and K.-F. Liu, *Phys. Rev. D* **96**, 114504 (2017), 1705.05849.
- [39] R. G. Edwards and B. Joo (SciDAC, LHPC, UKQCD), *Nucl. Phys. Proc. Suppl.* **140**, 832 (2005), [832(2004)], hep-lat/0409003.
- [40] M. Lüscher and S. Schaefer, *Comput. Phys. Commun.* **184**, 519 (2013), 1206.2809.
- [41] D. Djukanovic (2016), 1603.01576.